

**PRELIMINARY DUMAND SITE EVALUATIONS:  
MAUI BASIN AND KEAHOLE POINT BASIN**

**ROBERT R. HARVEY**  
and  
**JAMES E. ANDREWS**  
HAWAII INSTITUTE OF GEOPHYSICS

**J. RONALD ZANEVELD**  
SCHOOL OF OCEANOGRAPHY  
OREGON STATE UNIVERSITY  
CORVALLIS, OREGON

JUNE 1978

Supported by  
NOAA, OFFICE OF SEA GRANT, GRANT 04-6-158-44114;  
OFFICE OF NAVAL RESEARCH,  
CONTRACT N00014-67-A-0369-0007, PROJECT NR 083-102;  
NOAA MUST PROGRAM; HIG; and  
MARINE AFFAIRS COORDINATOR'S OFFICE, STATE OF HAWAII

**HAWAII INSTITUTE OF GEOPHYSICS**  
UNIVERSITY OF HAWAII



Preliminary DUMAND Site Evaluations:

Maui Basin and Keahole Point Basin

Robert R. Harvey  
and

James E. Andrews

Hawaii Institute of Geophysics

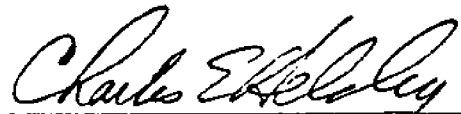
J. Ronald Zaneveld

School of Oceanography  
Oregon State University  
Corvallis, Oregon

June 1978

Supported by

NOAA, Office of Sea Grant, Grant 04-6-158-44114;  
Office of Naval Research,  
Contract N00014-67-A-0369-0007, Project NR 083-102;  
NOAA MUST Program; HIG; and  
Marine Affairs Coordinator's Office, State of Hawaii



Charles E. Helsley  
Director,  
Hawaii Institute of Geophysics



*ABSTRACT*

*The proposed DUMAND project requires construction of a photomultiplier/hydrophone array comprising a cubic kilometer of seawater at 5 kilometers depth on the ocean bottom. Such an unprecedented scale of deep ocean engineering requires detailed knowledge of the environmental parameters which will affect the deployment, operation and maintenance of the system. This report describes the findings of a preliminary survey of geological, geophysical, water current and optical characteristics at the two proposed Hawaiian sites: Maui Basin and Keahole Point Basin.*



## TABLE OF CONTENTS

Abstract. . . . .	iii
List of Figures . . . . .	vii
List of Tables. . . . .	viii
 INTRODUCTION. . . . .	 1
PRELIMINARY GEOLOGICAL INVESTIGATIONS OF DUMAND SITES . . . . .	4
James E. Andrews	
Keahole Point, Hawaii . . . . .	10
 PRELIMINARY BOTTOM CURRENT SURVEY OF THE MAUI BASIN AND KEAHOLE POINT SITES . . . . .	 19
Robert R. Harvey	
Introduction. . . . .	19
Description of Measurements . . . . .	19
Implications for DUMAND . . . . .	25
Conclusions . . . . .	26
 PRELIMINARY OPTICAL SURVEY OF THE MAUI BASIN AND KEAHOLE POINT SITES . . . . .	 28
Ronald Zaneveld	
Introduction. . . . .	28
Instrumentation . . . . .	32
Free Vehicle Instrument Package . . . . .	32
Experimental Results. . . . .	34
Discussion. . . . .	37
Implications for DUMAND . . . . .	38
 ACKNOWLEDGMENTS . . . . .	 42
 REFERENCES. . . . .	 43



## List of Figures

<u>Figure</u>	<u>Page</u>
1. Ship tracks Mn 76-01, Maui Basin, showing slope break. . . . .	5
2. Profile A, B (see Fig. 1) . . . . .	6
3. Profile C, D, E (see Fig. 1). . . . .	7
4. Shear strength profiles for Maui Basin cores. . . . .	11
5. Characteristic linear regression curve for Maui Basin shear strength. . . . .	12
6. Bathymetry off Keahole Point after H. O. Chart 4102 . . . . .	13
7. Bathymetry off Keahole Point from HIG cruise tracks . . . . .	14
8. Seismic reflection profile on central track of Fig. 7 - northern segment. . . . .	16
9. Seismic reflection profile on central track of Fig. 7 - central segment . . . . .	17
10. Seismic reflection profile on central track of Fig. 7 - southern segment. . . . .	18
11. Bathymetric chart of the southeastern Hawaiian Islands, showing station locations for coring, CTD, transmissometer, and current meters. . . . .	20
12. Free vehicle current meter package. . . . .	22
13. Time series of bottom currents recorded off Keahole Point, Hawaii. . . . .	23
14. Time series of bottom currents recorded southeast of Hawaii . . . . .	24
15. Sketch of OSU optical deep-moored C-meter . . . . .	33
16. Maui Basin profiles: transmission, $\sigma_T$ , temperature and salinity . . . . .	35
17. Keahole Point profiles: transmission, $\sigma_T$ , temperature and salinity. . . . .	36



List of Tables

<u>Table</u>		<u>Page</u>
1.	Dumand Site - Critical Environmental Uncertainties. . . . .	2
2.	Current Knowledge of Proposed Hawaiian Dumand Sites . . . . .	3
3.	Physical Properties of Dumand Site Cores - MN 76-01 . . . . .	9
4.	Observed Transmittance and Attenuation Coefficient, and Theoretical Scattering Coefficient for Pure Water . . . . .	30
5.	Measured and Calculated Optical Parameters. . . . .	41

## INTRODUCTION

The DUMAND (Deep Underwater Muon and Neutrino Detector) project proposes to study muon and neutrino interactions at ultra-high energies and to investigate astronomical phenomena via "neutrino light". The proposed technique involves creating a vast target-detector consisting of  $1 \text{ km}^3$  of seawater ( $10^9$  tons) at a deep ocean location. Using the natural shielding of the ocean above to filter unwanted noise from the abundant lower energy interactions, a three-dimensional array of photomultipliers and hydrophones will detect Cerenkov light and acoustic signals generated by particle cascades. The signatures of these cascades will lead to identification of incoming ultra-relativistic muons and neutrinos.

The huge hydrophone/photomultiplier array and the deep ocean technology required lead to cost estimates which demand detailed engineering design before launching the project. This involves both design of a practical array and careful evaluation of the relevant environmental parameters at proposed sites. Parameters of interest are presented in Table 1.

Two candidate sites in Hawaii have been selected on the basis of available knowledge of these criteria and logistic considerations. They are the Maui Basin, north of Kahului, Maui, and the Keahole Point Basin, west of Keahole Point, Hawaii. This report presents the results of a preliminary study of these sites, and reviews our present knowledge concerning their optical clarity, deep ocean currents and bottom characteristics. Table 2 summarizes this information.

TABLE 1

## DUMAND SITE -- CRITICAL ENVIRONMENTAL UNCERTAINTIES

PARAMETER	IMPACT ON DUMAND EXPERIMENT
Optical Clarity	Number, Spacing and Calibration of Optical Sensors
Bioluminescence	1. Optical Sensor Noise Levels, False Alarms and Sophistication of Data Processing 2. (Indirectly) Same for Acoustic Sensors
Acoustic Background Noise	Noise Levels, False Alarms and Data Processing
Biofouling/Sedimentation	Acoustic Noise Levels and Degradation of Optics
Deep Ocean Currents	Spacing, Bracing and Directivity of Array
Nepheloid Layer	Requirement for "Tare" or Excess Array Height
Bottom Characteristics	"Clearing" Time After Deployment, Plus Choice of Weight Versus Stake-Down Anchor Technique
Offshore Slopes	Route, Length and Risk for Cable Deployment

TABLE 2

## CURRENT KNOWLEDGE OF PROPOSED HAWAIIAN DUMAND SITES

Site	Maui	Keahole Point
Depth-maximum	5740 m	4900 m
Depth-basin closure	5500 m	4500 m
Area of basin within closure	$\sim 1300 \text{ km}^2$	$\sim 1000 \text{ km}^2$
Sediment thickness	>750 m	>250 m
Sediment type	siliceous  brown silty clay-- large island-derived fraction	Northern Basin-siliceous  Southern Basin-brown clay
Sediment acoustic character	highly reflective  acoustically	north 50-100 m trans. layer  south reflective, acoustically stratified
Sediment shear strength	$5-20 \text{ g/cm}^2 @ 1 \text{ m}$	unknown
Currents	unknown	$4 \text{ cm/sec}^*$
Light attenuation	small nepheloid layer and sill effect $\sim 400 \text{ m}$ thick	no nepheloid layer

\* peak recorded over 8 days

## PRELIMINARY GEOLOGICAL INVESTIGATIONS OF DUMAND SITES

By James E. Andrews

Maui Basin

Maui basin, originally proposed as the prime array site by the Site Selection Committee at the 1976 DUMAND Summer Workshop, lies at the base of the island slope north-northeast of the island of Maui. The basin as defined by the 5500-m contour is 75 km (40 n.m.) long and 18 to 28 km (10 to 14 n.m.) wide. All areas within this contour lie within 100 km (60 n.m.) of Kahului, Maui, the principal commercial center of the island. The basin was visited for a brief reconnaissance survey during 1976 by the R/V KANA KEOKI on cruise Mn-76-01. Fig. 1 shows the ship track over the landward portion of the basin. Greatest depths, encountered at the base of the island slope, were between 5710 and 5740 m. The island slopes approaching the basin (Figs. 2 and 3) are between 7° and 12°; slopes on the basin floor are on the order of 0.3°. The basin slopes upward to the north-northeast away from the island slope base, and toward the Hawaiian Arch. Seismic profiles over the basin and lower slope show acoustically well-stratified sediment accumulations up to 750 m in the basin. Available core data show the sediment to be an interbedded sequence of biogenic oozes, clays, and island-derived turbidite layers. Up to 250 m of local ponding has occurred on ledges near the slope base. It is not possible to determine sediment cover on the steeper sections of the slope. The reflection profiles at both high (80-600 Hz) and low (10-80 Hz) frequencies show the basin sediments acoustically well stratified; strong reflections suggest significant island-derived input to the sediment column.

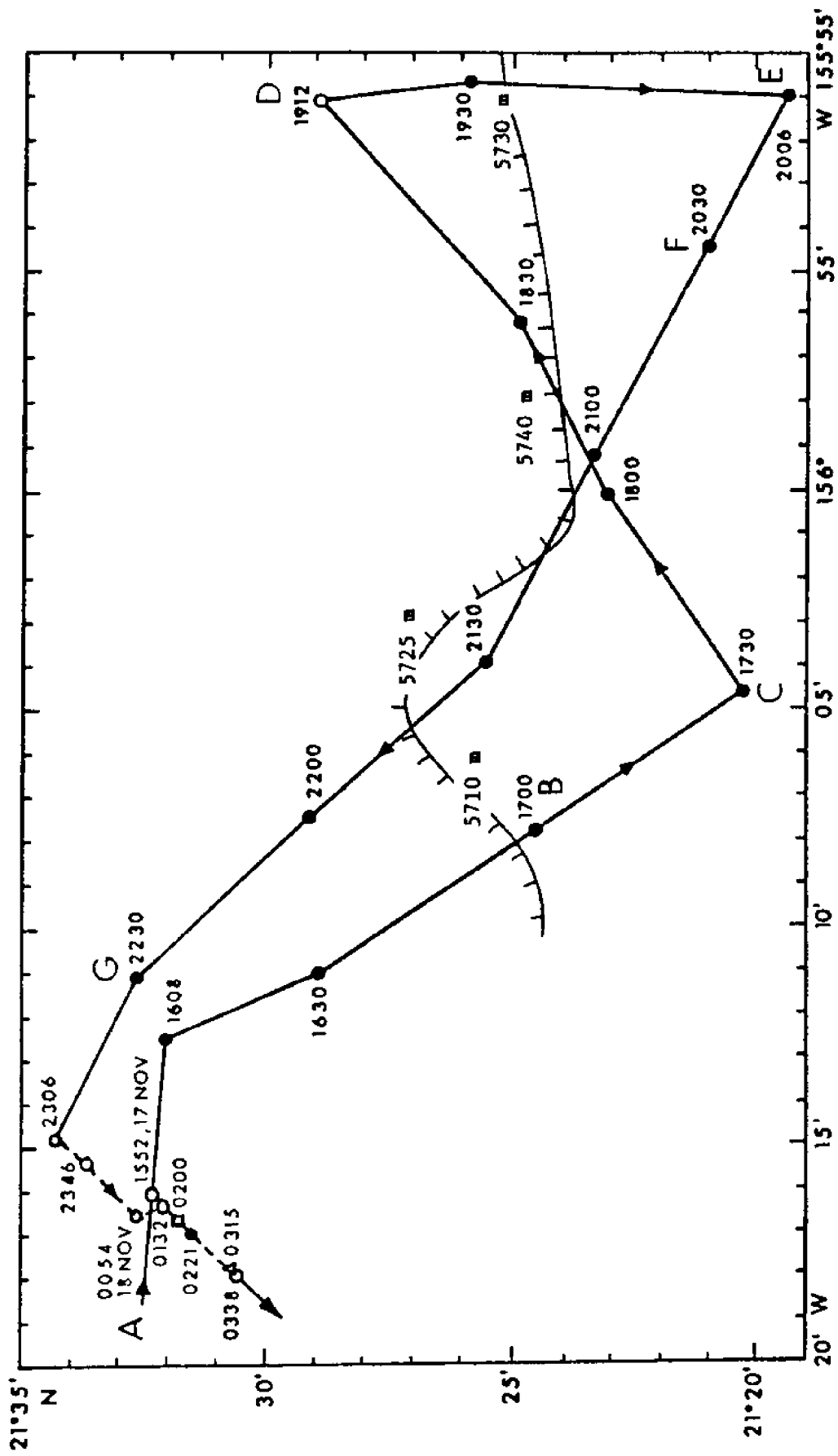


Fig. 1. Ship tracks Mm 76-01, Maui Basin, showing slope break.

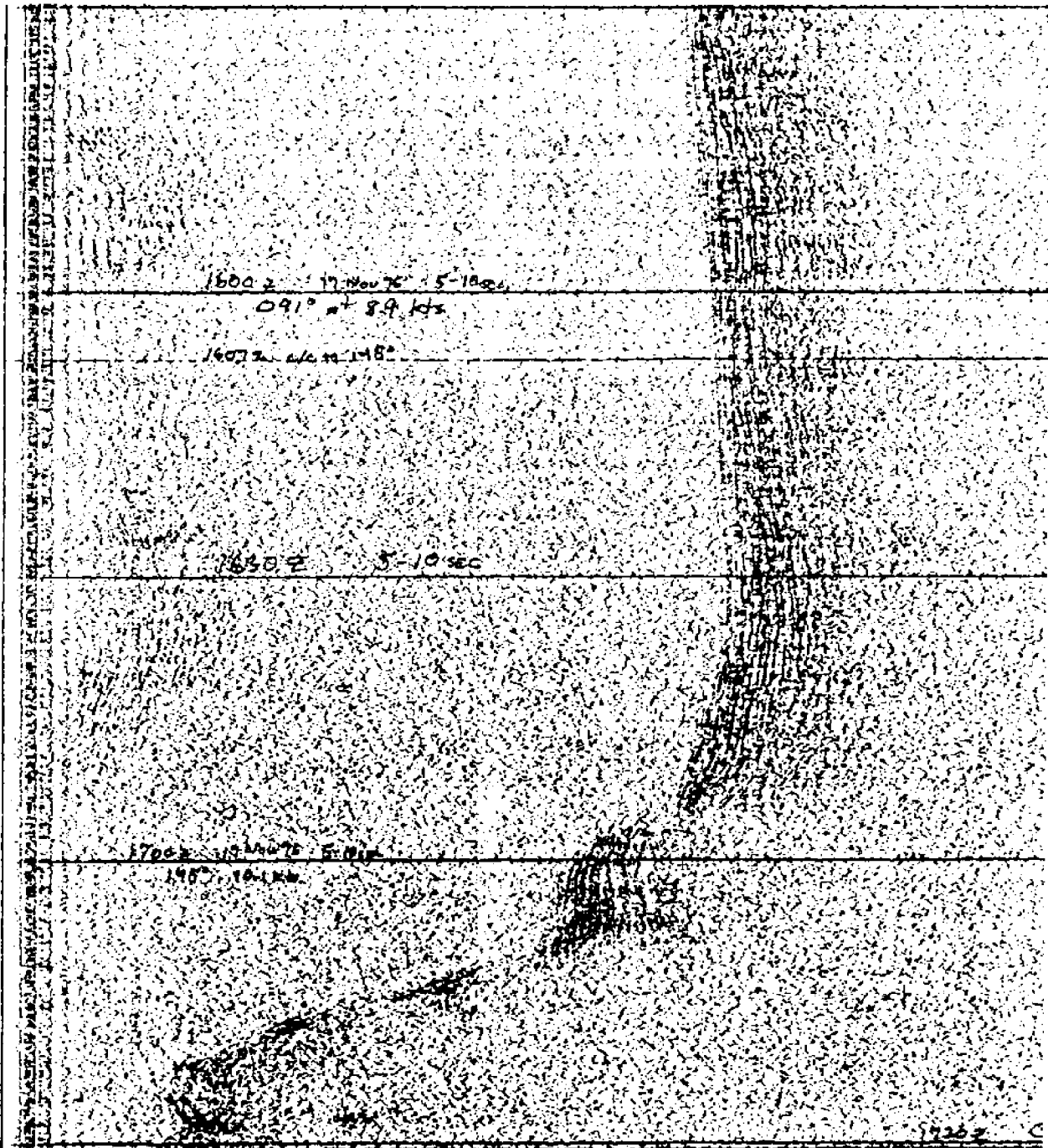


Fig. 2. Profile A, B (see Fig. 1)

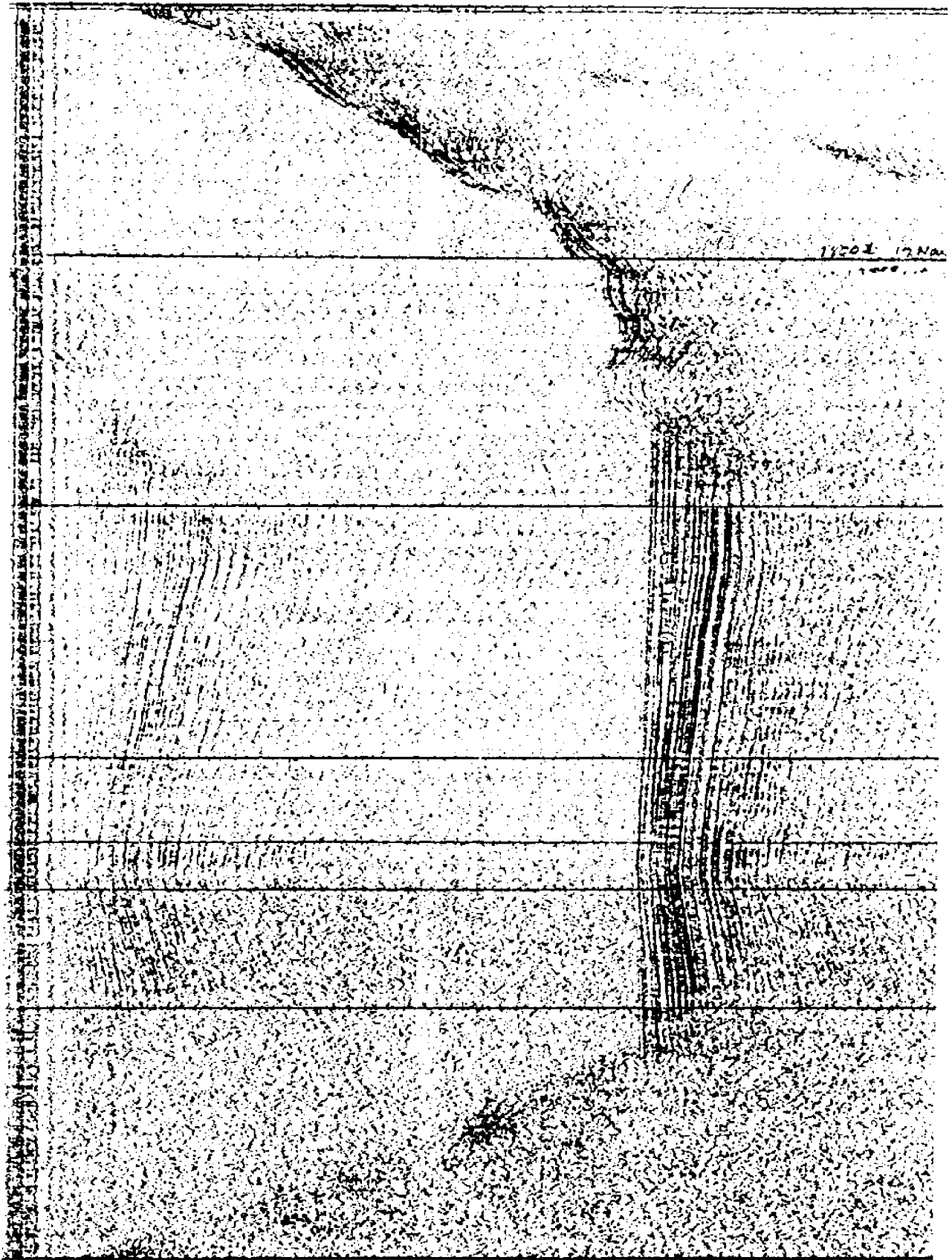


Fig 3. Profile C, D, E (see Fig. 1)



Three Benthos-type freefall corers were used to obtain sediment samples for description of stratigraphy and physical properties. Cores were recovered from the NW sector of the basin at a depth of 5640 m. The coring operations were located by a satellite navigation fix at 21°31.61'N, 145°16.49'W, and all cores were recovered within an area of approximately  $\pm 100$  m of this position. The sediment cores recovered were 77.5 cm (FFC-D), 81 cm (FFC-A), and 96 cm (FFC-B) in length and consisted of a dark brown silty clay with thin black layers. The uppermost 10-15 cm were severely disturbed in the coring process. A characteristic visual description is as follows:

- (1) 10-20 cm dark brown (10YR 3/3) silty clay with a thick (5-m) layer of fine terrigenous (olivine/pyroxine) black sand;
- (2) 20-60 cm dark brown (10YR 3/2) silty clay with several thin (1-cm) layers of fine terrigenous black sand;
- (3) 60-90 cm yellowish brown (10YR 5/4) mottled silt.

Table 3 summarizes mass physical property measurements made by the HIG core lab one month after core recovery. Following the Mn-76-01 cruise, the cores were stored in an upright position at room temperature. The sampling technique (freefall gravity coring) and storage procedures used create some uncertainty in the values reported in Table 3, although the water content and sensitivity values agree with other data for this sediment type. Values for bulk density, however, are approximately 40% lower than characteristic values, which could be due to inaccuracies in the porosity-plug subsampling methods used. Values for shear strength are also lower than expected, because of the coring method, which deforms the sediment on impact.

TABLE 3

## PHYSICAL PROPERTIES OF DUMAND SITE CORES - MN 76-01

	W	D	T <sub>max</sub>	T <sub>rem</sub>	St
Max.	180	1.32	23.0	6.1	8.0
Min.	146	1.08	7.40	1.5	2.6
Mean	166	1.16	13.6	3.25	4.98
Std. Dev.	11.1	0.07	4.40	1.49	1.80
Samples	11	11	42	10	10

W = water content % dry weight

D = unit weight or bulk density

T<sub>max</sub> = maximum shear strength before deformation

T<sub>rem</sub> = remolded shear strength

St = sensitivity (T<sub>max</sub>/T<sub>rem</sub>)

Fig. 4 shows the shear strength profiles ( $T_{\max}$  and  $T_{\text{rem}}$ ) for the three cores measured at 5-cm intervals. Fig. 5 shows a characteristic shear strength curve obtained by linear regression. Note that values steadily increase down-core to an extrapolated value of  $26 \text{ g/cm}^2$  at 1-m depth. The remolded strength curve shows a slightly decreased strength dependence on depth. Shear strength was measured by fallcone penetration with a Geonor instrument and accompanying calibration tables.

These measurements provide an initial description of the surficial sediments of Maui Basin, although inadequacies in sampling recovery and storage cause some uncertainty in the reported values. Future mass physical property investigations should emphasize obtaining undisturbed samples and testing them immediately upon recovery. Piston coring and in situ strength testing would provide a more reliable description of the upper sedimentary section of this site.

#### Keahole Point, Hawaii

The basin off Keahole Pt., Hawaii lies at the base of the slope west of the island. The basin has a maximum width of 75 km (40 n.m.) due west of Keahole Pt., but the presence of Indianapolis Seamount in the center of the basin restricts the area useful for DUMAND purposes. The useful portion of the basin lies east and northeast of the seamount and follows the base of the island ridge to the northwest. This basin has not been the subject of preliminary work except for nephelometer stations. The general outline of the basin is shown in Fig. 6 after HO chart 4102. A compilation of data from the HIG data bank has permitted rough contouring of general bathymetry (Fig. 7). The greatest depth indicated is over 4940 m

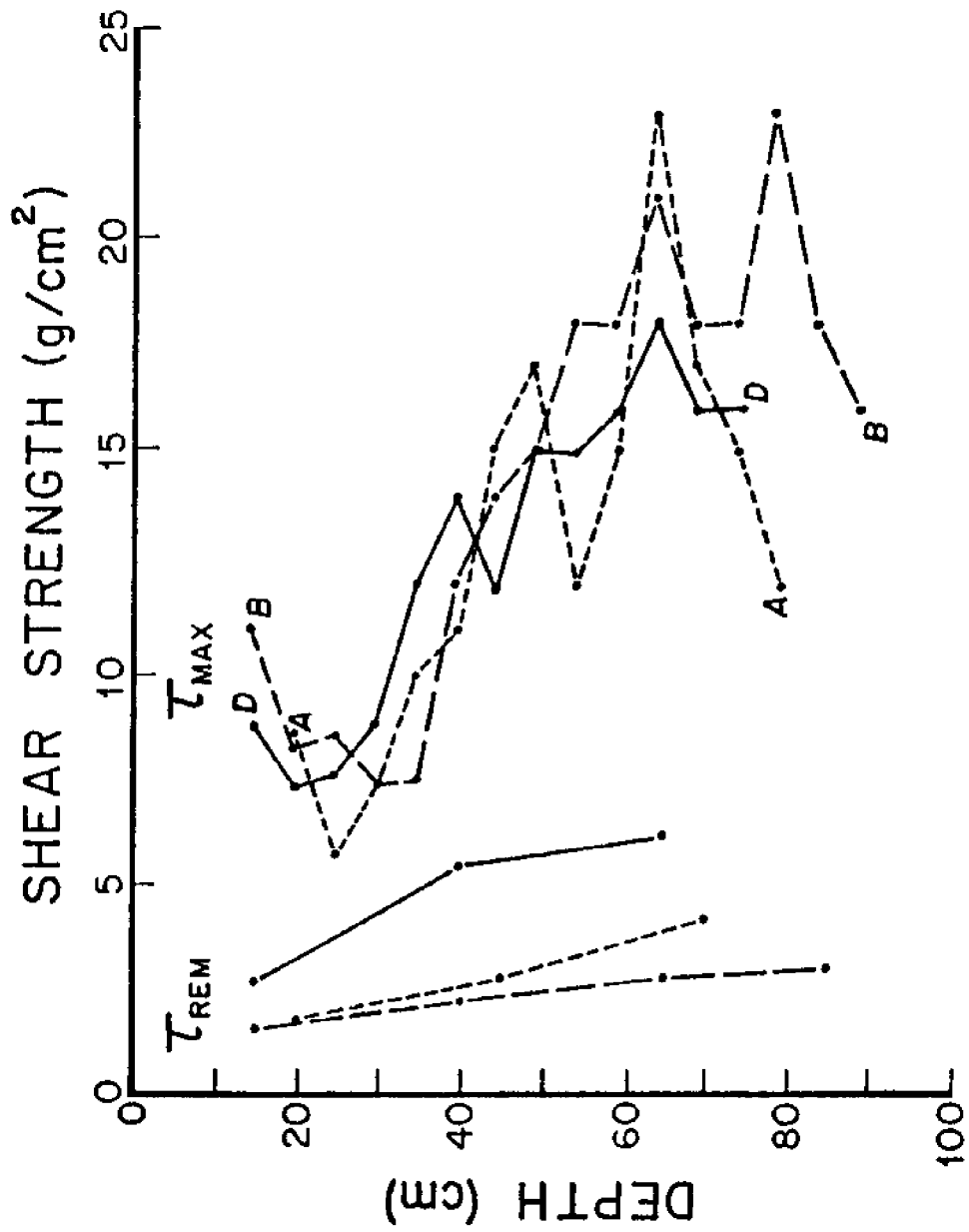


Fig. 4. Shear strength profiles ( $T_{max}$  and  $T_{rem}$ ) for Maui Basin cores.

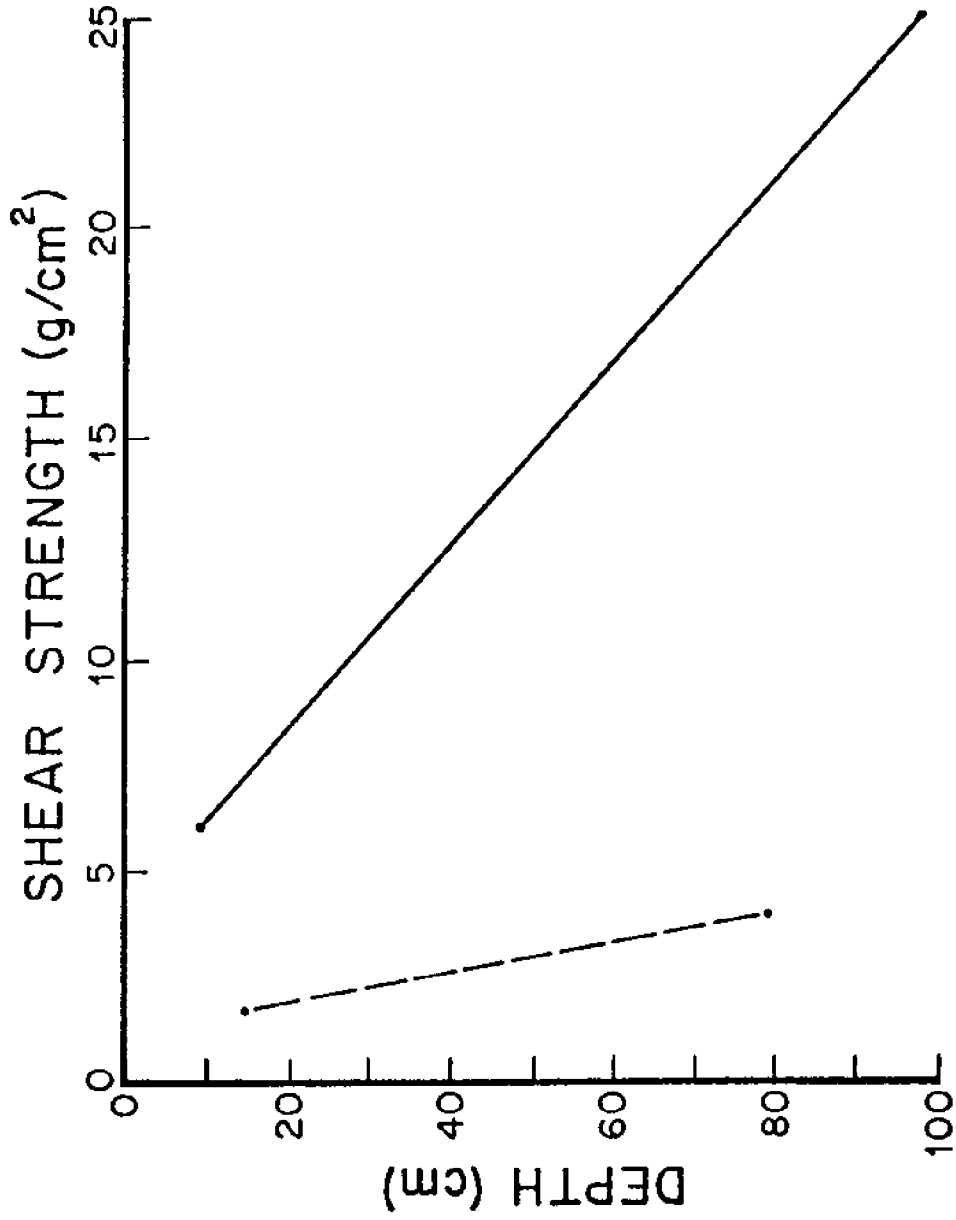


Fig. 5. Characteristic linear regression curve for Maui Basin shear strength.

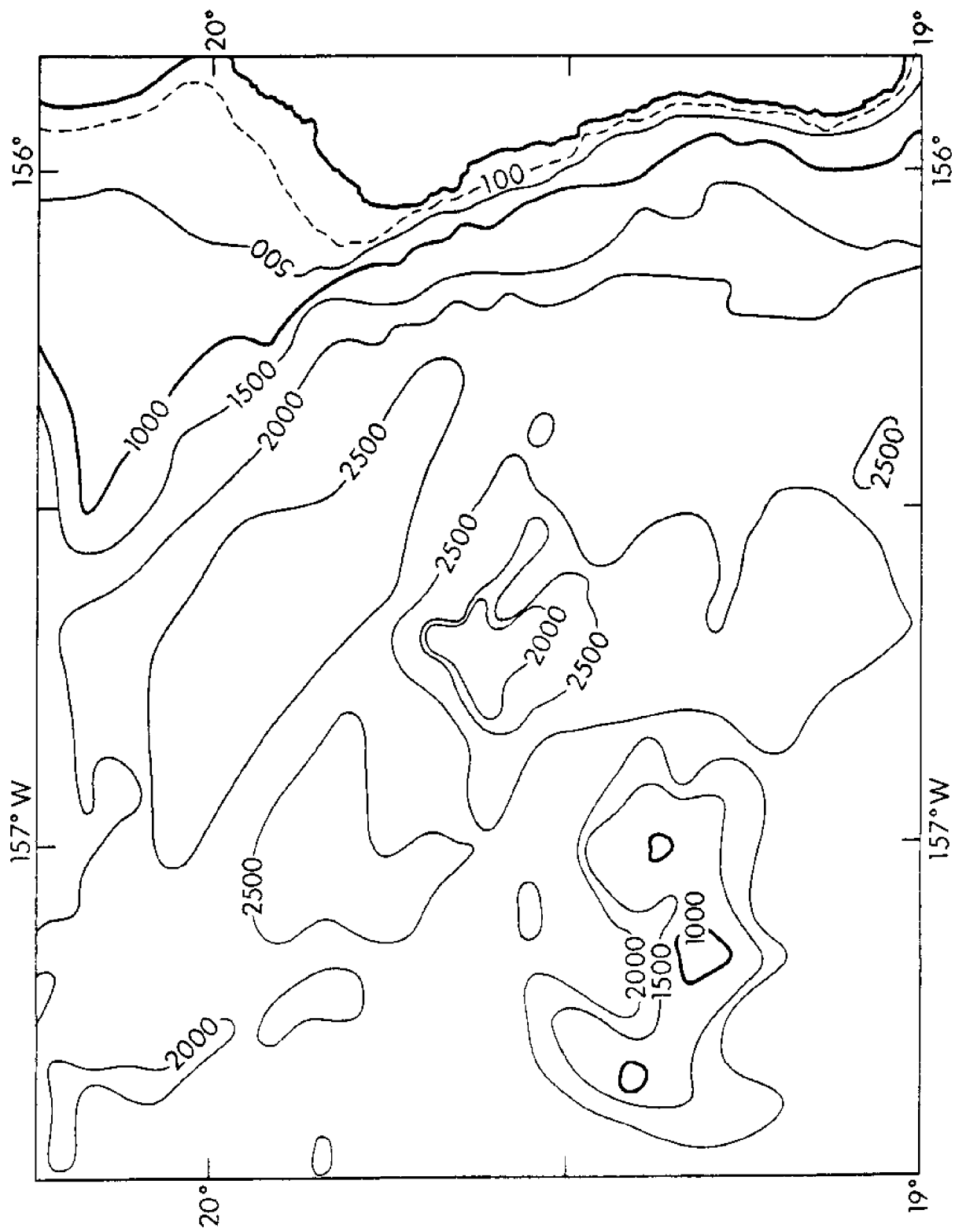


Fig. 6. Bathymetry off Keahole Point after H.O. Chart 4102.

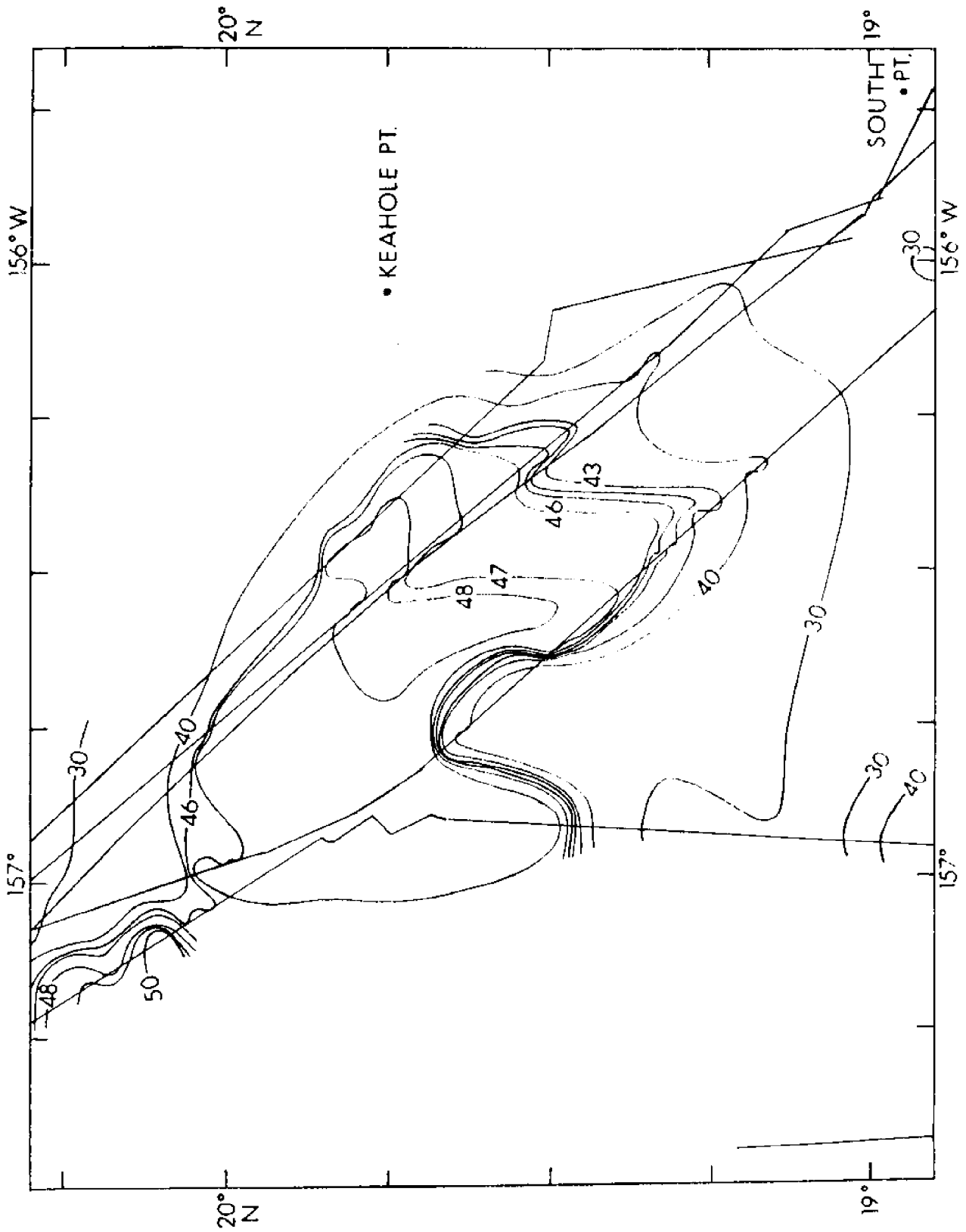


Fig. 7. Bathymetry off Keahole Point from HIG cruise tracks.

(2700 fm) on the HO chart, and over 4800 m on the HIG track lines. The portion of the basin of interest is elongate in the northwest direction, and its greatest depth is toward the west.

Seismic reflection data were recorded on one of the HIG tracks across the westernmost part of the basin. Segments of this line are illustrated in Figs. 8, 9, and 10. The basin surface appears to be nearly flat on this line (running south-southeast). Of particular interest is the acoustic response of the sediment column. In contrast to the Maui site, which showed a strong surface reflectivity and acoustically well-stratified sediments to at least 750-m depth, the Hawaii basin has in its northern half a 50- to 100-m layer of acoustically transparent sediments overlying acoustically stratified sediments. In the southern portion of the basin the acoustically stratified sediments are exposed at the seafloor. It appears that the northern portion of this basin may be more restricted in terms of circulation and input of island-derived sediments than either the Maui Basin site or the southern portion of the Keahole Basin. It is also possible that high productivity produced by mixing of wind-driven surface waters passing through Alenuihaha Channel and forming an eddy between Hawi and Keahole may produce the localized sedimentation maximum that appears as the transparent layer.

The accumulation of such a biogenic section suggests the possible advantage of quiet bottom conditions for the array. On the other hand, it might also present disadvantages such as very slow clearing rates for the array volume when the soft bottom sediments were disturbed, and noise problems and high fouling associated with the high productivity.



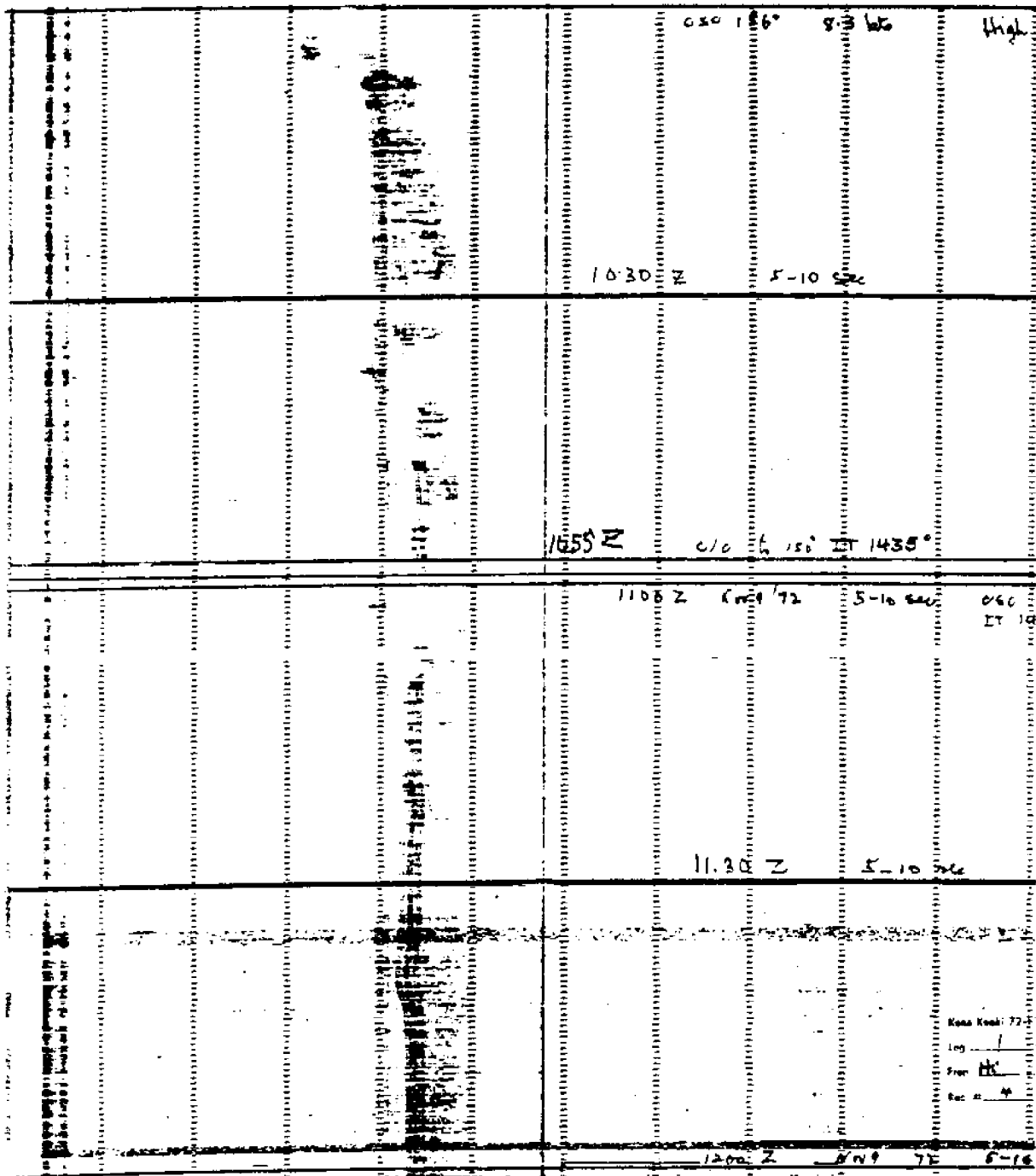


Fig. 8. Seismic reflection profile on central track of Fig. 7 - northern segment.

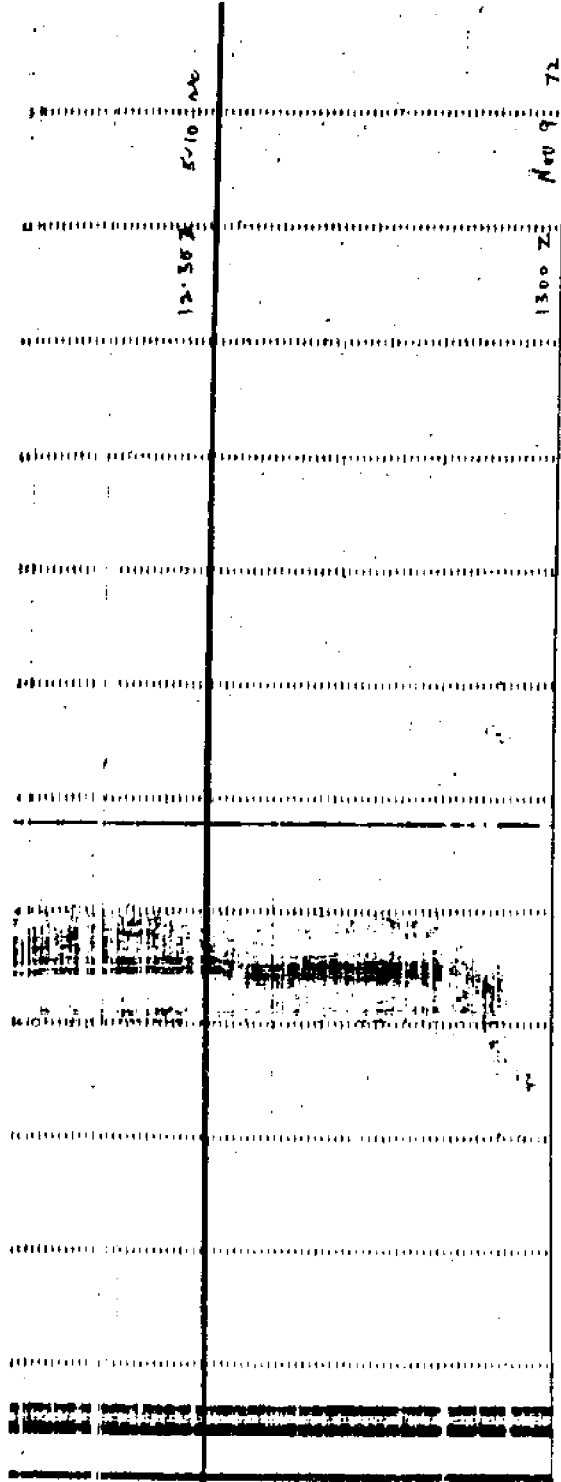


Fig. 9. Seismic reflection profile on central track of Fig. 7 - central segment.

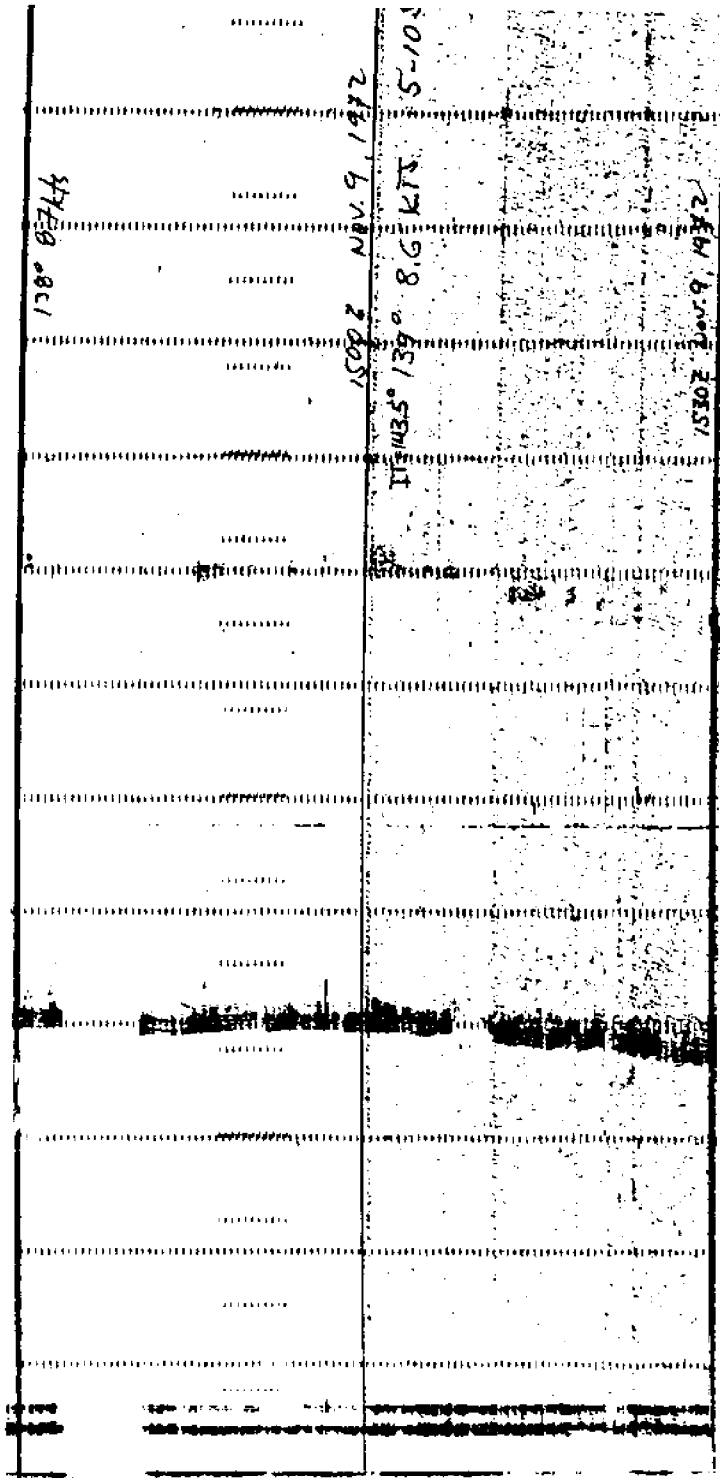


Fig. 10. Seismic reflection profile on central track of Fig. 7 - southern segment.

PRELIMINARY BOTTOM CURRENT SURVEY OF THE MAUI BASIN AND KEAHOLE POINT  
SITES

By Robert R. Harvey

Introduction

Deep bottom currents in the vicinity of the Hawaiian Archipelago are virtually unknown. Considerable information is available on the surface current regime, which is dominated by baroclinic motion and thus gives no clue to the deep circulation.

Currents can be either directly measured with a current meter, which provides an Eulerian time history at a single point, or they may be inferred from observations of physical and chemical seawater properties. The latter technique necessarily implies a long-term average, so that all information on temporal variability is lost. For the purposes of determining site suitability for DUMAND, we are concerned chiefly with the peak current to be encountered at the array location, so that the temporal variability is critical.

Description of Measurements

We report here on two deep water, bottom current measurements in the vicinity of the Hawaiian Islands. We know of no other examples. One such measurement was made in support of an ocean bottom seismometer study, south of the island of Hawaii. The second was deployed in the Maui Basin expressly for the DUMAND site survey. Station locations are shown in Fig. 11.

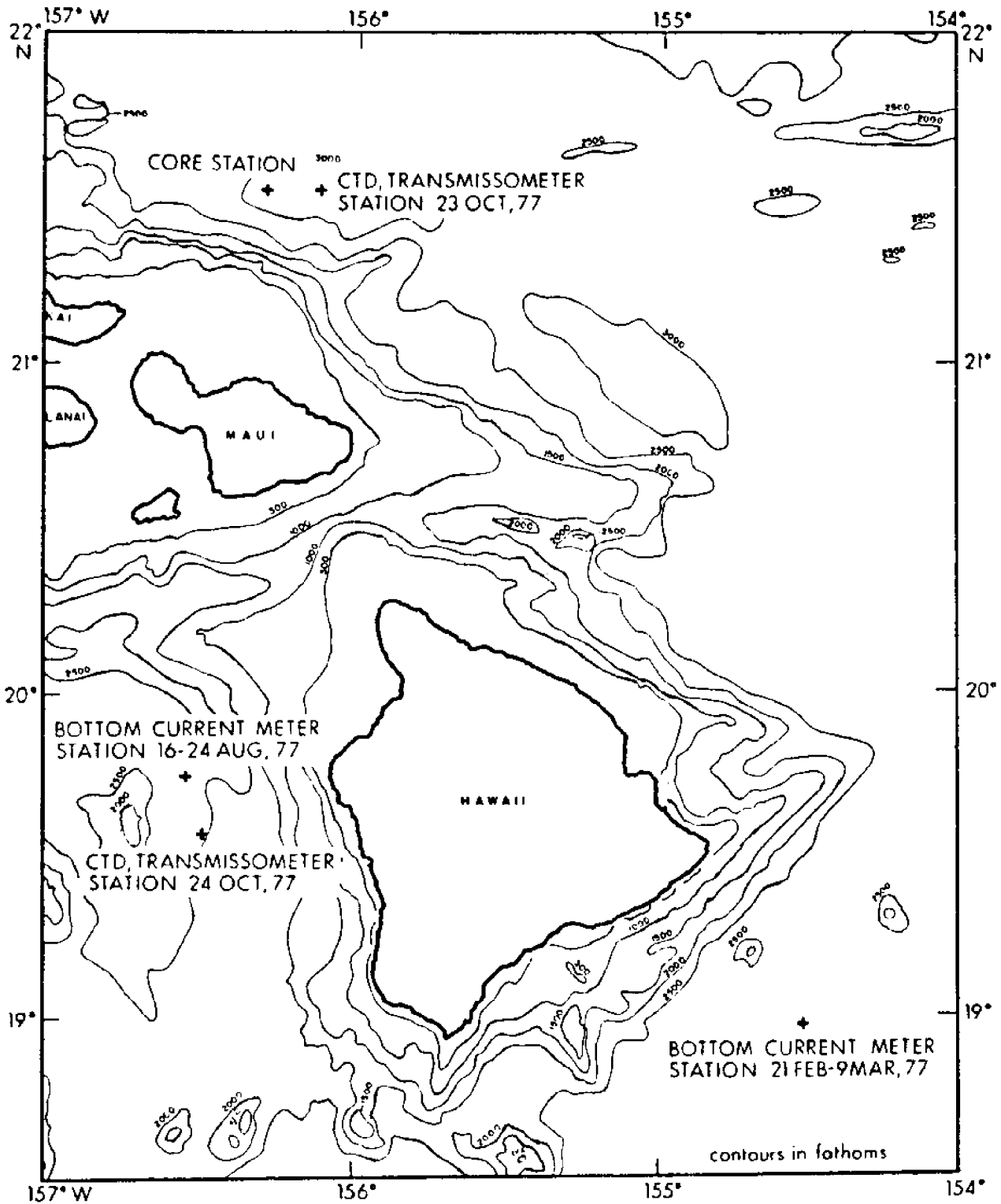


Fig. 11. Bathymetric chart of the southeastern Hawaiian Islands, showing station locations for coring, CTD, transmissometer, and current meters.

The instrument configuration is the same for both measurements and is shown in Fig. 12. The current meter is launched as a free vehicle package. The entire assembly sinks to the ocean floor, leaving the current meter 30m from the bottom and out of the boundary layer. After a preset time on the release units, an explosive bolt severs the anchor from the current meter and the package ascends. On the surface the radios are activated, allowing us to locate and retrieve the current meter.

The current meters are Geodyne model 102 type, which have been modified from the original film recording scheme to digital magnetic tape cassette recording (Nakamura and Harvey, 1978). Rotor counts, inclination, and vane and compass directions are sampled every minute. These data are then vector averaged and decimated to one-hour intervals, and VECPLOT, a statistical and plotting program for vectorial data (D. Halpern, pers. comm.), is applied to display the results, shown in Figs. 13 and 14.

Both records are typical of deep ocean currents, in that tidal oscillations of about 2-to 3 cm/sec amplitude dominate the steady currents. These oscillations cause the east-west and north-south components to pass through a slack water period almost every day. Peak current speeds south of Hawaii reached 9 cm/sec, whereas those off Keahole Point were only about 4 cm/sec. Note, however, that the "steady" current (neglecting tidal oscillations) south of Hawaii was about 1 cm/sec to the east from Feb. 21 to Feb. 27, when suddenly it became northerly at 4 cm/sec. Such events, possibly benthic storms, have been observed many times in deep ocean current records.

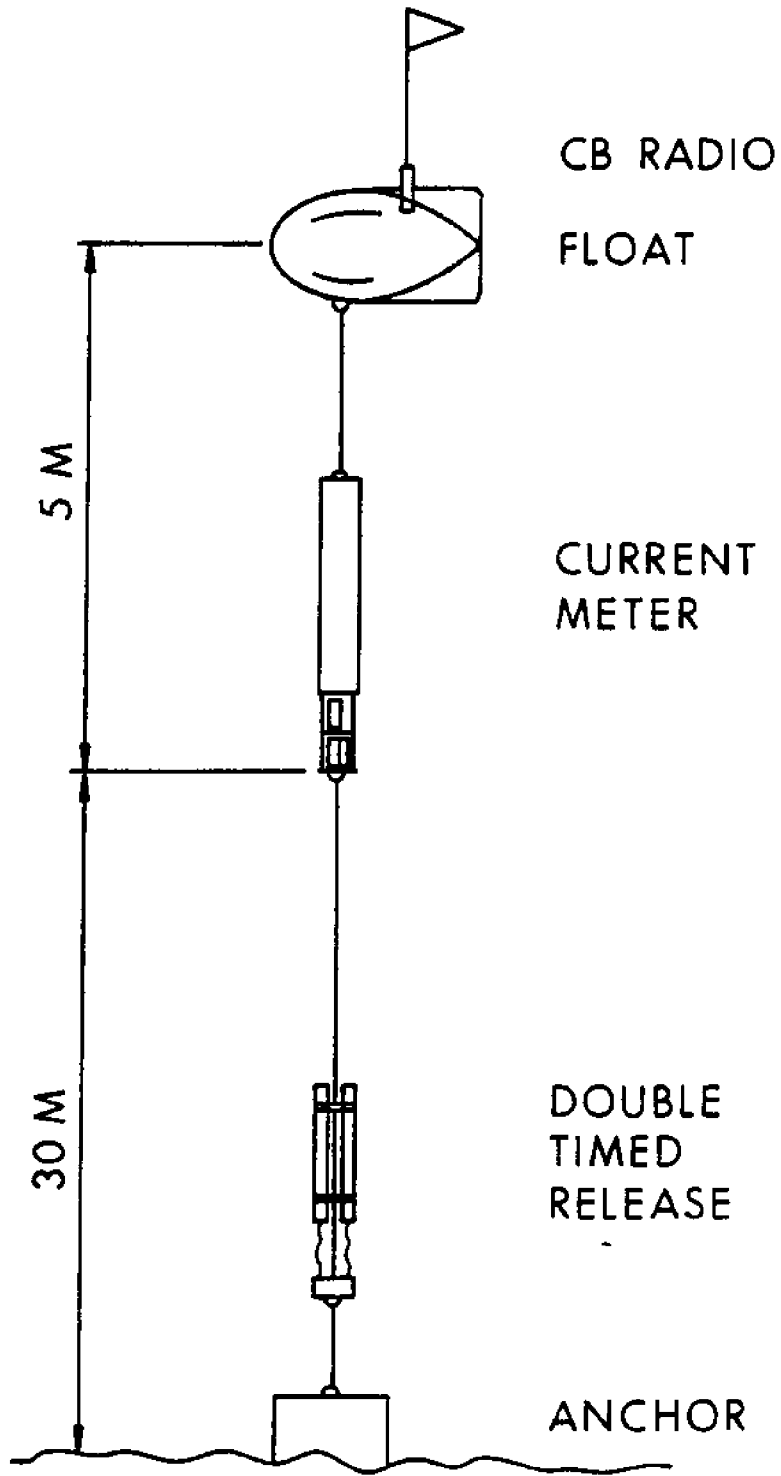


Fig. 12. Free vehicle current meter package.

TIME SERIES OF VECTOR AVERAGED CURRENTS AT #J156 KEAHOLE PT  
 LOCATION = LAT 19 44.5N, LONG 156 30.3W, DEPTH = 4788 METERS  
 OBSERVATION PERIOD = 1200 16 AUG 77 TO 1700 24 AUG 77 ( 8.3 DA  
 AVERAGING INTERVAL = 1.0 HOURS ( 1 POINTS)

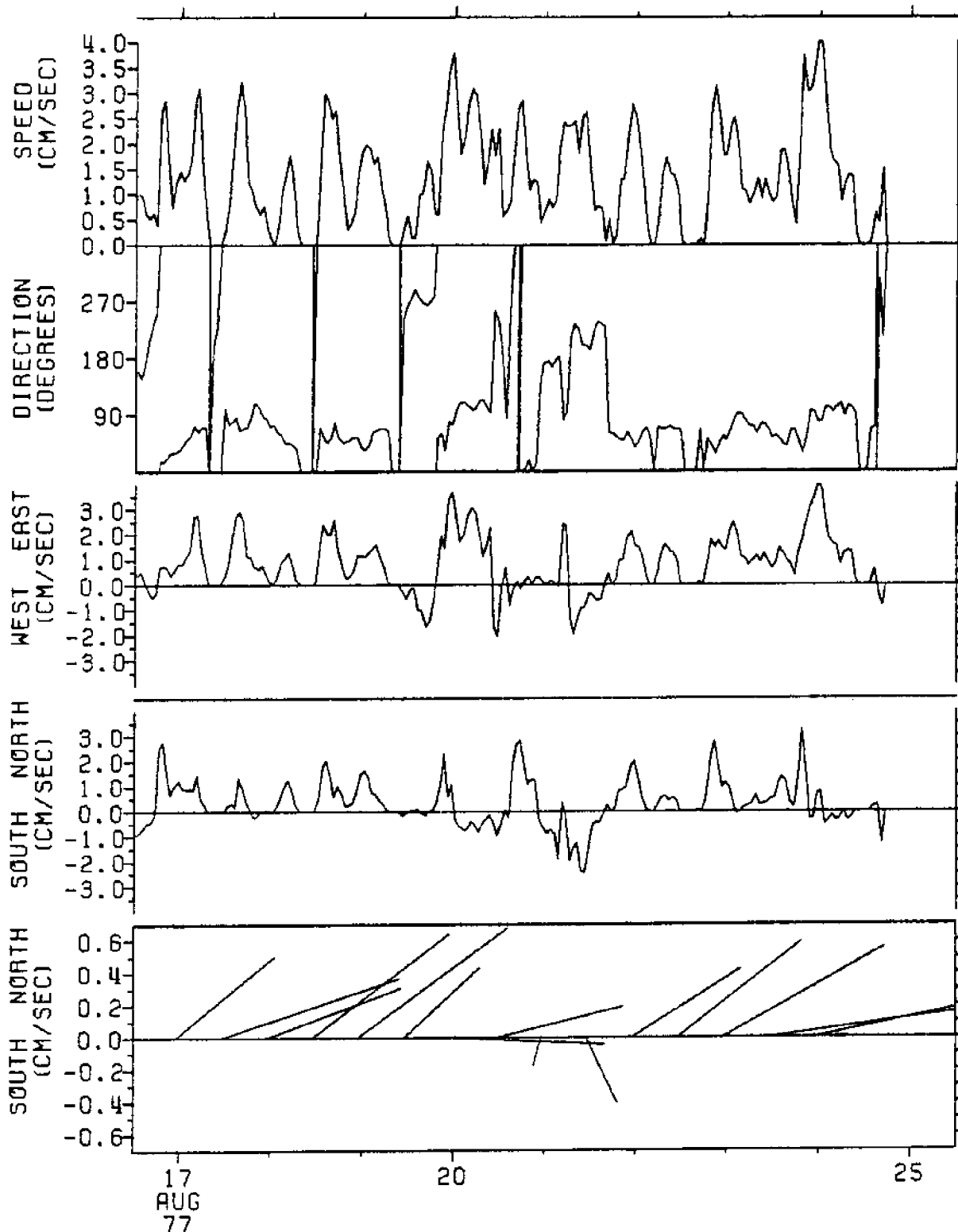


Fig. 13. Time series of bottom currents recorded off Keahole Point, Hawaii. From top to bottom are shown the current speed, current direction, east-west component, north-south component, and stick vectors. The upper four traces are based on hourly averages; the bottom trace represents 12-hour averages.



TIME SERIES OF VECTOR AVERAGED CURRENTS AT CM#459 OBSSHI  
 LOCATION = LAT 18 58.6N, LONG 154 30.9W, DEPTH = 5300 METERS  
 OBSERVATION PERIOD = 1200 21 FEB 77 TO 0100 9 MAR 77 ( 15.6 DA  
 AVERAGING INTERVAL - 1.0 HOURS ( 1 POINTS)

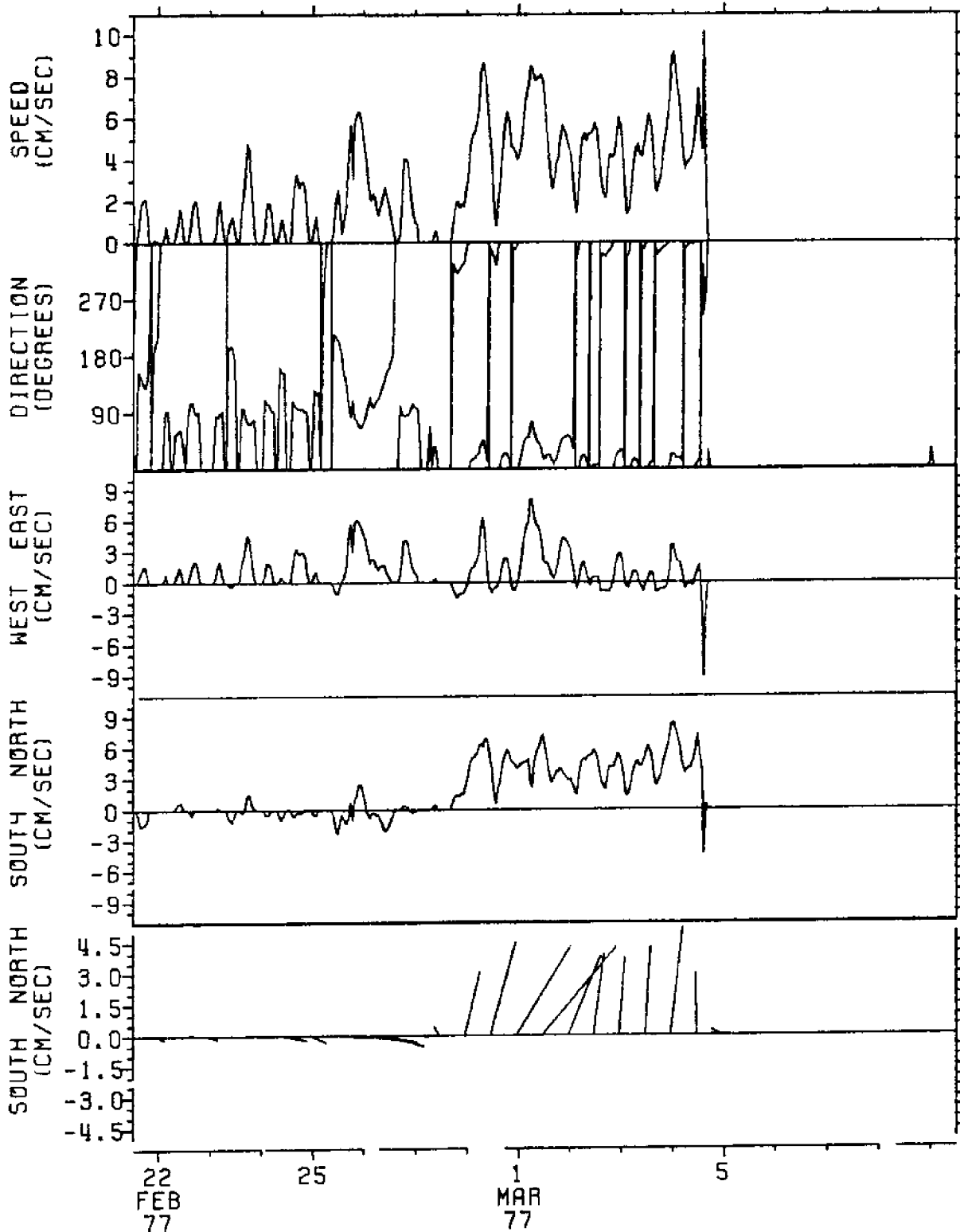


Fig. 14. Time series of bottom currents recorded southeast of Hawaii. From top to bottom are shown the current speed, current direction, east-west component, north-south component, and stick vectors. The upper four traces are based on hourly averages; the bottom trace represents 12-hour averages.

### Implications for DUMAND

Excessive current can interfere with DUMAND success in three ways:

- 1) by physically disturbing the deployed array,
- 2) by stirring bottom sediment into suspension to interfere with detection and,
- 3) by maintaining this material in suspension as a bottom nepheloid layer.

Direct physical effects of currents upon the DUMAND array will obviously depend on the specific design. This design will be partly based on the site survey results, and will incorporate the available current information.

Erosion of bottom sediments generally requires a current of 15 to 50 cm/sec, depending on the sediment characteristics. Transporting this sediment and maintaining it in suspension require considerably less current speed. Thus a rapidly varying current, whose average speed may be low but whose peaks are sufficient to stir up the sediment, may maintain a nepheloid layer.

For DUMAND site criteria, we are interested chiefly in the current speed, shown in the upper traces of Figs. 13 and 14. The maximum current observed during the 20 days of recording at the two sites reached only 9 cm/sec, insufficient to generate a nepheloid layer. The tidal contribution to these currents can be assumed to be limited to a few cm/sec amplitude for all time. However, non-periodic variations in the 'steady' current, such as those due to benthic storms, may introduce far stronger currents.

Using temperature profiles and hydrographic data, Edmond et al. (1971) traced bottom currents across the Central North Pacific. They concluded that the main flow of Bottom Water between the central and northeast Pacific basins is carried by a narrow current, less than 400 m thick, which sweeps the southern shore of Hawaii and turns north; the edge of this northerly flow crosses the Maui Basin. This suggests that a meandering of the main flow could cause long term variations in the currents observed at that site.

In addition, one of Edmond et al.'s high-precision temperature profile stations, Zetes 82, was located just east of the Maui Basin. This cast showed the characteristic regional profile with a minimum at mid-depth and an adiabatic gradient to deep water. However, from 4800 m to the bottom at 5200 m an anomalous temperature decrease appeared, producing a secondary maximum at about 4800 m. Edmond et al. attribute this inflection to the injection of cold bottom water in the bottom 400 m. The present CTD cast north of Maui also was characterized by a step in salinity and light transmissivity about 400 m above the bottom, which could also be associated with this bottom current passing through the Maui Basin.

### Conclusions

Direct bottom current measurements have been made at only one proposed DUMAND site (Keahole Point) and only for about one week. This record shows a benign current environment in that the peak observed speed reached only 4 cm/sec, which is insufficient to generate a nepheloid layer or to disturb a reasonable DUMAND array. At the other proposed site, in the Maui Basin, no direct current observations have yet been made.

However, high-precision temperature profiling indicates a strong current over the bottom 400 m which sweeps the south coast of Hawaii and turns north, its western edge just passing across the Maui Basin. An 11-day bottom current record from the southeast tip of Hawaii shows an easterly 1 cm/ sec current for the first seven days, suddenly turning north at 4 cm/sec for the remaining four days. This non-stationary character may be indicative of meandering or strength fluctuations in the bottom current, which could similarly affect the Maui Basin site. Direct current measurements of longer duration are needed at both sites.

## PRELIMINARY OPTICAL SURVEY OF THE MAUI BASIN AND KEAHOLE POINT SITES

By J. Ronald Zaneveld

Introduction

The two optical processes that govern the distribution and intensity of light in the oceans are scattering and absorption. Scattering is the redistribution of light without loss of intensity. Absorption is a process in which light energy is turned into another form of energy, resulting in a decrease in light intensity.

The absorption coefficient,  $a$ , is defined as the internal absorption of an infinitesimally thin layer of the medium normal to a light beam, divided by the thickness of the layer. The total scattering coefficient,  $b$ , is defined similarly. The beam attenuation coefficient,  $c$ , is then defined by:

$$c = a + b \text{ (units of } m^{-1}\text{)}.$$

Attenuation is thus simply the sum of scattering and absorption. Furthermore, the transmission of a well-collimated beam of light,  $T(z)$ , is then given by:

$$T(z) = e^{-cz},$$

where  $z$  is the light path transversed. The directional properties of light scattering are given by the volume scattering function,  $\beta(\theta) = \frac{dI(\theta)}{E dV}$ , where  $dI(\theta)$  is the radiant intensity emanating from a volume element  $dV$  when it is illuminated by irradiance  $E$ . The total scattering coefficient  $b$  is related to  $\beta(\theta)$  by:

$$b = 2\pi \int_0^\pi \beta(\theta) \sin \theta \, d\theta.$$

For a review of the optical properties of the ocean see Jerlov (1976).

In order to assess the relative clarity of a given water sample one needs a reference point. Unfortunately, attenuation values for pure water are not well known. Table 4 summarizes the current state of knowledge. It is likely that even Sullivan's transmission values are too large. The problem is to totally exclude stray light from the receiver. Furthermore, the attenuation of pure water is primarily an absorption process. For the optical instruments used in this study one may also obtain a value for the attenuation of pure water by extrapolation, when both the particle concentration and attenuation are known. For the measurements made with the instrument used in this study, this results in a transmittance for pure water of 66.5% at 650 nm compared to 70.4% and 75.0% in Table 4.

The light attenuation in the visible region of a sea water sample is due to absorption and scattering by water itself, to absorption of dissolved humic acids (the so-called 'yellow matter'), and to absorption and scattering of particulate matter. The effect of dissolved salts is negligible. The yellow matter absorbs strongly at the short wavelengths, but the absorption decreases exponentially with increasing wavelength. In the red spectral region, absorption of yellow matter may be ignored. The wavelength dependence of attenuation by suspended particulate matter is more or less proportional to  $1/\lambda$  (Morel, 1973). Generally, particulate scattering is much larger than absorption. In the deep ocean, optical attenuation components of primary concern are attenuation due to water and particulate scattering, since

TABLE 4

OBSERVED TRANSMITTANCE AND ATTENUATION COEFFICIENT,  
AND THEORETICAL SCATTERING COEFFICIENT FOR PURE WATER

Wavelength (nm)	Transmittance (% m <sup>-1</sup> )		Attenuation coefficient (10 <sup>-3</sup> m <sup>-1</sup> )			Scattering coefficient (10 <sup>-3</sup> m <sup>-1</sup> )
	1	2	1	2	3	
375						
400	95.6		45			7.68
425	95.8		43			5.81
450	96.8		33			4.47
475	98.1		19			3.49
500	98.2		18			2.76
525	96.5		36			2.22
550	96.0		41			1.79
575	93.3		69			1.49
600	91.3	89.7 (580 nm)	91	109 (580 nm)		1.25
625	83.3	75.2	186	272		1.09
650	79.6	73.7	228	305		
675	75.0	70.4	288	351		
700	69.3	64.5	367	438		
725	60.7	52.3	500	648		
750	29	17	1,240	1,750		
775	9	7	2,400	2,680		
800	9	7	2,400	2,630		
	18		2,050			

1 = Clarke and James (1939); 2 = Sullivan (1963); 3 = Morel (1974).

the absorption due to yellow matter in the deep ocean is probably small (Zaneveld, 1973; Ivanoff, 1973). The light attenuation by particulate matter depends on the concentration, size distribution, shape distribution, and index of refraction distribution of the suspended particulates (see for example, Morel, 1973; Zaneveld et al., 1974; Jerlov, 1976). If the nature of the particulate matter is relatively constant in a given oceanic region (this is a reasonable assumption in the deep ocean), a simple relation between particle concentration and light attenuation can be experimentally determined (Kitchen et al., 1975). The optical parameters that were measured in connection with DUMAND have already been discussed in Zaneveld (1975) and Zaneveld (1976). These papers also discuss the small amount of optical and particle data in existence before the measurements described in this paper were taken. A primary requirement of DUMAND is high optical clarity over long periods of time.

Optical elements of the DUMAND array will be able to detect not only directly transmitted light, but also some near-forward scattered light. The light reaching a detector in the array from an event a distance  $x$  away has been attenuated by a factor of approximately  $e^{-\eta x}$ , where  $\eta$  is given by:

$$\eta = c - 2\pi \int_0^{\theta'} \beta(\theta) \sin \theta \, d\theta.$$

$\theta'$  is the acceptance angle of the photomultiplier. Because  $\beta(\theta)$  is sharply peaked in the forward direction, it becomes important to measure this parameter at small angles. This can be done either directly with water samples from hydrocasts or by calculation since it has recently been shown that Mie's (1908) theory is correct for oceanic particulates in the near-forward region (Spinrad et al., 1978).



Determination of  $\eta$  is of major concern to DUMAND because an attenuation length may be defined as  $\frac{1}{\eta}$ . The volume concentration of optical array elements, and hence cost, is proportional to  $(\frac{1}{\eta})^3$ .

### Instrumentation

The transmissometer used in this study has a light-emitting diode source with a wavelength of 650 nm. The source is pulsed, with a synchronous photodiode detector. The detector and source are in the same housing; and light path is folded by means of a porro prism. The output of the LED is also constantly monitored by a photodiode with the same characteristics and electronics circuit as the other photodiode. The output of the instrument is given as the ratio of the light intensity that traversed the water to the directly measured LED intensity. The instrument is calibrated by setting the air transmission at 87.1%, which, due to different window reflectivities in air and in water, corresponds to 100% transmission in water. The output signal is recorded digitally on magnetic tape in a separate housing.

The accuracy of the temperature probe is approximately 0.005°C, whereas the salinity is accurate to within 0.03%.

### Free Vehicle Instrument Package

Both the CTD and nephelometer are usually deployed attached to a wire and lowered to the bottom by a winch. For the present measurements a large ship with winch capability was not available, so the instruments were reconfigured into an integrated free vehicle package, as shown in Fig. 15. The components of this package are launched in series, beginning

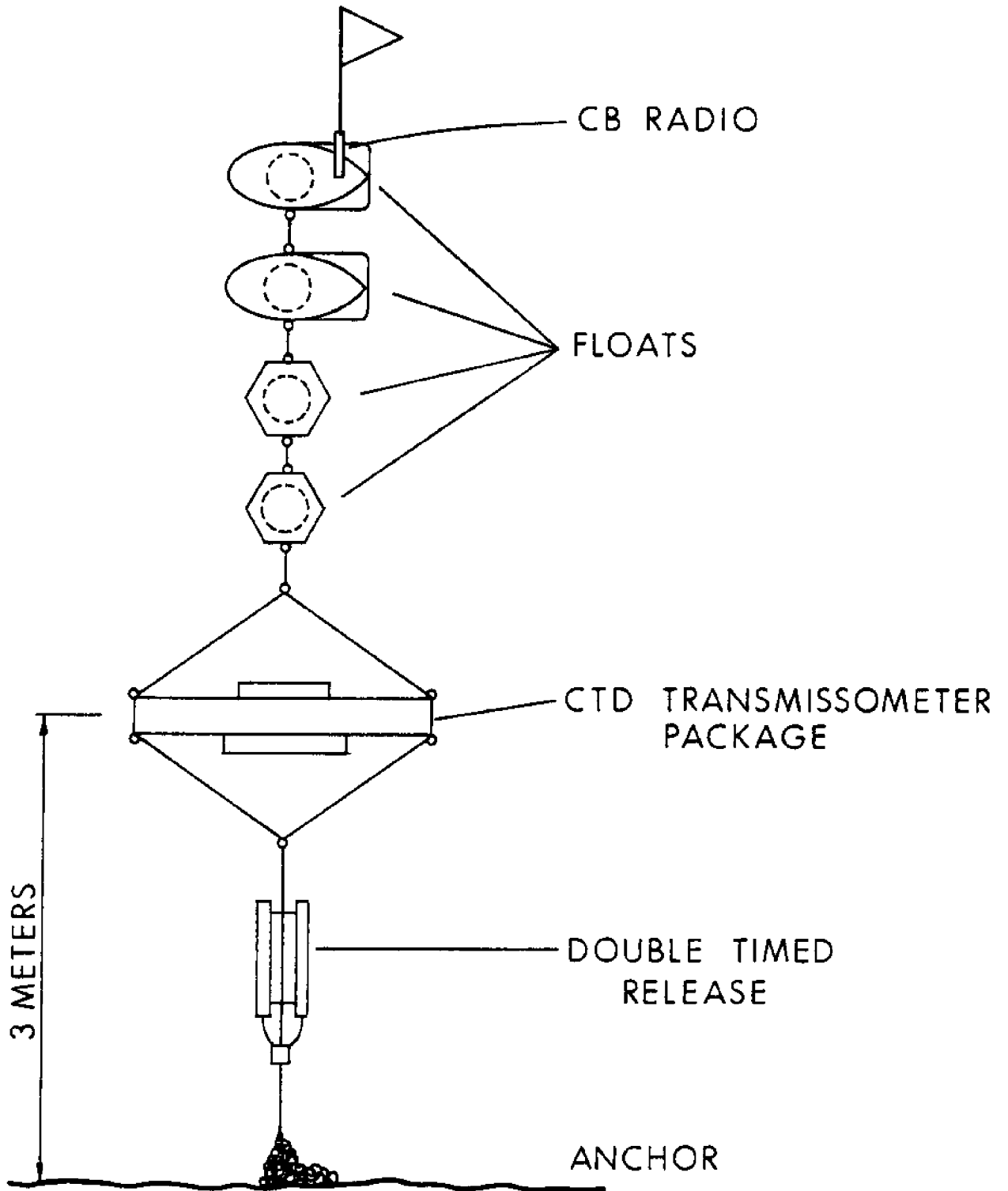


Fig. 15. Sketch of OSU optical deep-moored C-meter.

with the uppermost float. The lines connecting the components are long enough so that each one can be handled individually; thus the system can be launched by two men. When the anchor drops, the package falls to the bottom at 0.4 m/sec, recording temperature, conductivity, depth and light transmission during the descent.

The timed release is preset to release the anchor soon after touchdown, at which time the package ascends 0.9 m/sec, again recording all parameters. When it reaches the surface, pressure-deactivating switches on the radio beacons cause them to transmit, providing a homing signal and allowing location of the surfaced instrument. The system is then re-armed and the process repeated for subsequent profiles.

#### Experimental Results

An CTD-transmissometer cast was made in the Maui Basin on Oct. 23, 1977. Results are shown in Fig. 16. The surface layer is typically dirty, warm, and saline. A small relative salinity minimum between 300 and 650 m is accompanied by a transmission maximum. A temperature inversion occurs near the bottom of this layer. The transmission decreases steadily from 1000-m depth to the bottom at 5677 m. A salinity and density maximum exists 250 m above the bottom. The bottom 400 m also shows a transmission profile that decreases more rapidly than in the waters above.

The CTD-transmissometer cast off Keahole Point, Hawaii island was made on Oct. 24, 1977 (Fig. 17). The minimum salinity, maximum transmission layer does not exist off Hawaii. From 500 m to the bottom at 4733 m the salinity, temperature, and density profiles are virtually identical to those off Maui. The transmission is approximately 0.2% less than off Maui,

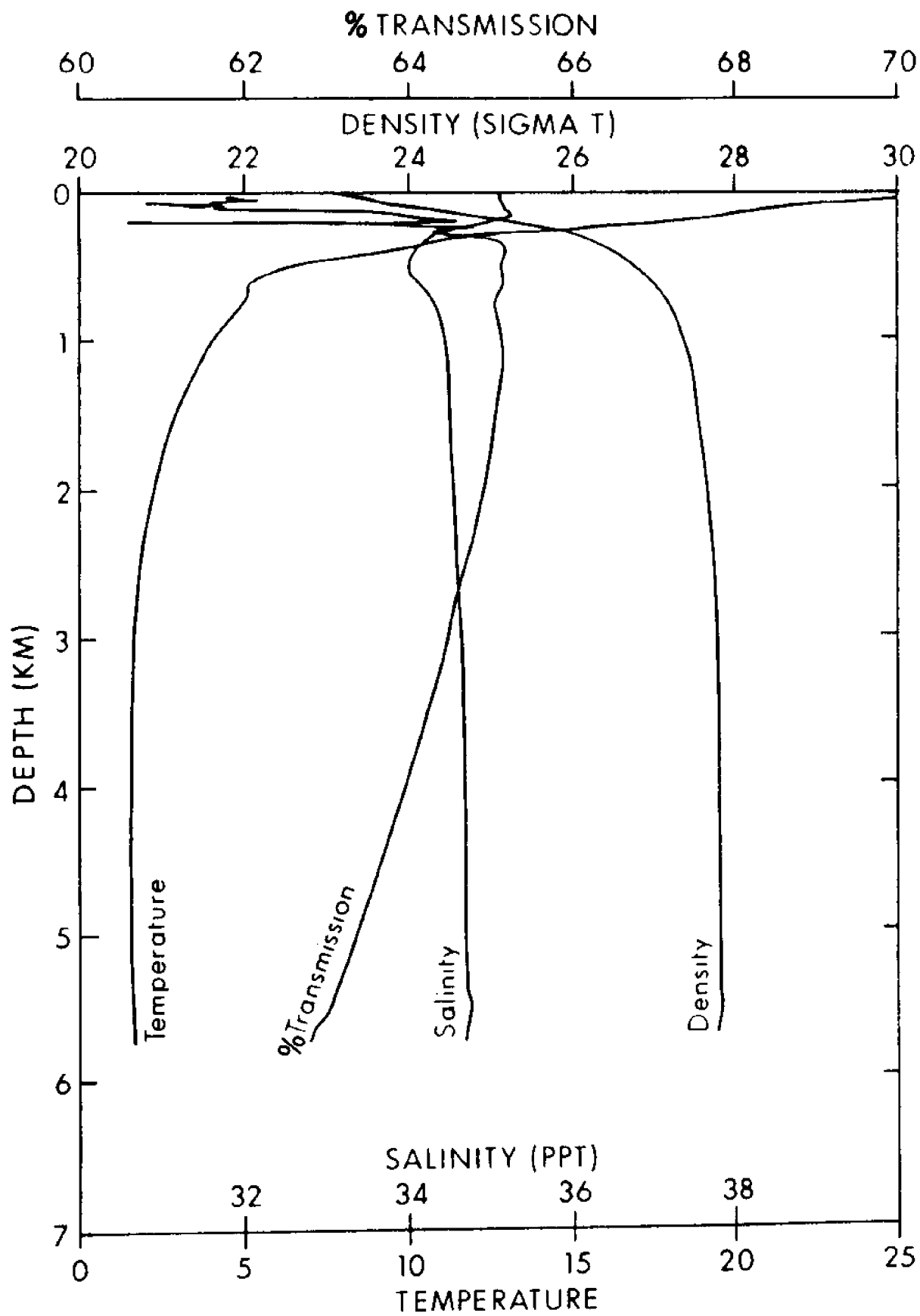


Fig. 16. Maui Basin profiles: % transmission,  $\sigma_T$ , temperature and salinity.

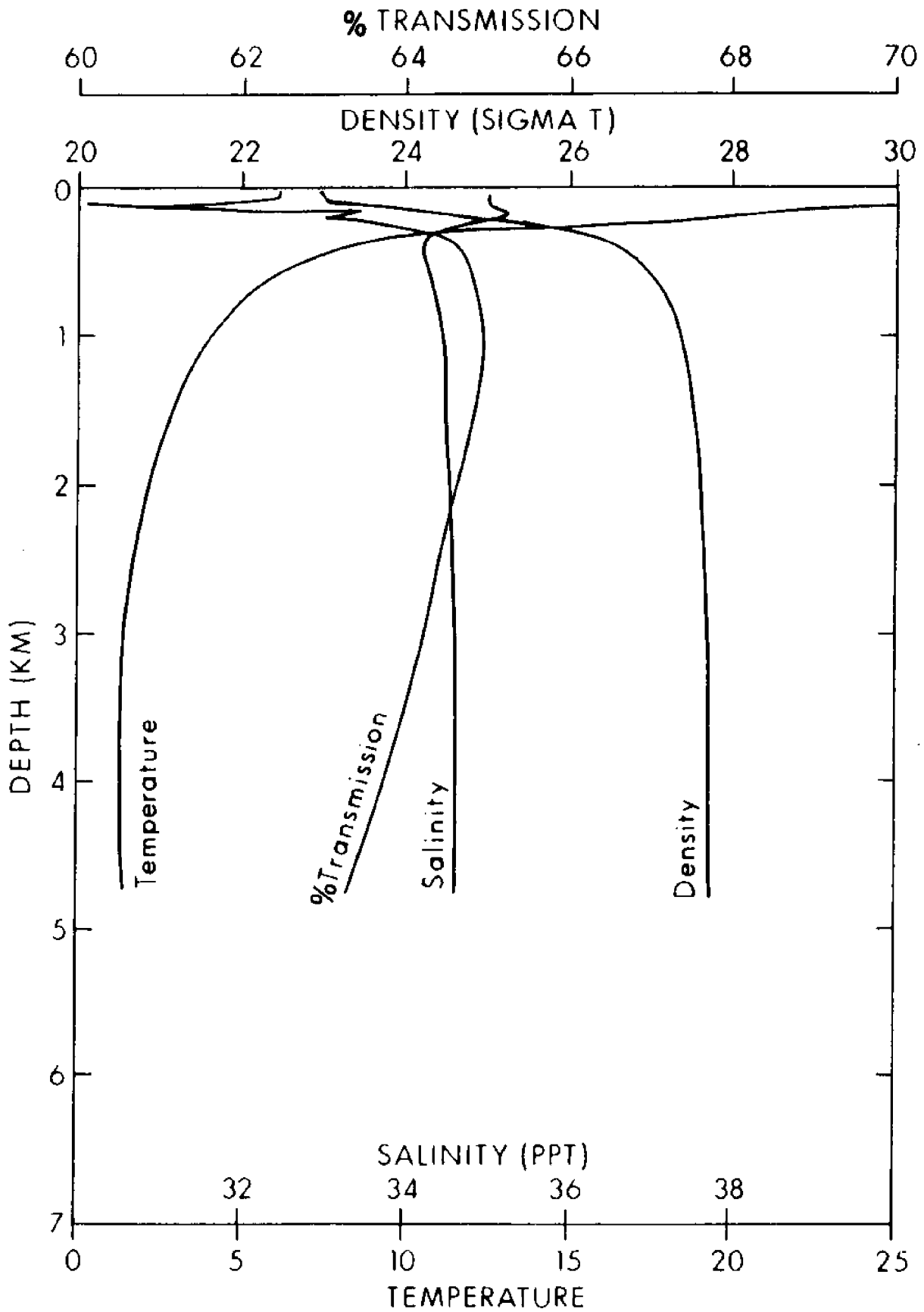


Fig. 17. Keahole Point profiles: % transmission,  $\sigma_T$ , temperature and salinity.

although the vertical rate of decrease is the same. No relative density maximum was observed near the bottom.

### Discussion

The most prominent feature of the optical profiles is the steady decrease in transmissivity with depth. Since high-resolution transmission profiles to large depths have only been made with this instrument, this feature was unexpected.

Initially it was feared that this decrease was an instrument problem due to pressure and/or temperature changes. Calculations and measurements indicate that no pressure problems exist, and cooling of the instrument to near-freezing did not alter the air calibration. One possible source of error that remains to be checked is non-uniform cooling of the instrument, which would result in different temperatures of the receiving photodiode and the LED-monitoring diode. Most of the transmissivity decrease can be explained by a number of physical processes, however.

The first of these processes is compressibility. Since sea water compresses at large depths, more water molecules are squeezed into the light path, and the absorption is increased. The change in volume of a parcel of sea water due to compression can be calculated (Defant, 1961). Using that number, we can calculate the increase in water molecules per unit volume. The attenuation coefficient can be expected to increase by the same percentage. By using the relation between the beam attenuation coefficient and transmissivity, we can then arrive at the change in transmissivity due to compression. At the Maui site, compression accounts for

0.56% transmission decrease, whereas at the Keahole site the decrease is 0.57% transmission.

The second process is the change in index of refraction of water as a function of temperature, salinity, and density. Tables have been prepared by Austin and Halikas (1976). Using measured parameters, we can then calculate the change in reflectivity of the glass-water interfaces of the transmissometer. This change accounts for approximately 0.4% transmission loss at both sites near the bottom.

The third factor is a possible larger concentration of particulate matter with increased depth. In the Maui cast a 0.4% transmission departure from the nearly linear decrease in transmissivity as a function of depth is apparent near the bottom. This departure is a nepheloid layer; the thickness of this layer is approximately 400 m, which corresponds well with the sill depth of the low ridge separating the two deep basins NE of Maui. Denser, less transparent water has apparently collected in the basin, where flushing appears minimal. At the Keahole Point site no near-bottom nepheloid layer is apparent. The steady increase in particle concentration must account for 0.5% transmission at the Keahole site and 0.8% transmission at the Maui site. While these numbers are not unreasonable in light of earlier observations (Lisitsyn, 1962; Plank *et al.*, 1972; Ewing and Connary, 1970); the remaining possible instrumental problem cannot be ignored.

#### Implications for DUMAND

The major concern to DUMAND is the attenuation-scattering length  $\frac{1}{\bar{\mu}}$ . As the increase in reflectivity of the windows due to the change of the index of refraction in the deep ocean does not affect the transmissivity,

this effect needs to be subtracted. Subtraction results in transmissivities and beam attenuation coefficient ( $a$ ) at 650 nm given in columns 1 and 2 on Table 5. The problem now is to use this measured figure and to estimate a value for  $1/\eta$ , the DUMAND attenuation length. In order to do so, we subtract from  $C(650)$  the component due to pure sea water,  $C_{\omega}(650)$ , to obtain  $C_{\rho}(650)$ , the particle attenuation coefficient. Since the Cerenkov radiation is predominant in the blue region of the spectrum, it is necessary to estimate the particle attenuation coefficient in the blue region. Because of selective absorption and scattering, the particle attenuation coefficient at 475 nm will be larger.

Jerlov (1974) has estimated that

$$(C-C_{\omega})_{355} = 1.8 (C-C_{\omega})_{650}$$

except perhaps for the cleanest waters. We thus underestimate the water clarity if we set in column 5,

$$(C-C_{\omega})_{475} = 1.8 (C-C_{\omega})_{650}.$$

By adding  $C_{\omega}(475) = 0.018 \text{ m}^{-1}$  to  $C-C_{\omega}$  we get  $C(475)$  in column 6 with units of  $\text{m}^{-1}$ . An attenuation length (units of m) is then obtained by calculation of  $1/C(475)$ . These attenuation lengths are very pessimistic, since the DUMAND array components will see scattered light as well. By assuming that the collection half-angle will be at least  $10^{\circ}$ , we find that we will gather at least 75% of the scattered light (Jerlov, 1976).

Furthermore, assuming that 80% of  $C-C_{\omega}$  is particle scattering, we obtain an upper limit for  $\eta$  from

$$\eta = C - 0.6(C-C_{\omega}).$$



This value is tabulated in column 8. The DUMAND attenuation length is then at least  $1/\eta$  m as shown in the last column of Table 5. The DUMAND attenuation length is 20 m or more, except near the bottom in the Maui Basin. It should be stressed that based on current understanding and measurements, these values are pessimistic. Direct measurements of spectral beam attenuation in the near future will resolve most of the uncertainties.

TABLE 5  
MEASURED AND CALCULATED OPTICAL PARAMETERS

	%Tr (650 nm)	C (650 nm)	C <sub>ω</sub> (650 nm)	C-C <sub>ω</sub> (650)	C-C <sub>ω</sub> (475)	C (475)	$\frac{1}{C(475)}$	$\eta(475)$	$\frac{1}{\eta(475)}$
Maui bottom (5676 m)	63.3	.465	.408	.057	.103	.121	8.3	.059	16.9
Maui 1000 m off bottom	64.0	.446	.408	.038	.068	.086	11.63	.045	22.2
Keahole bottom (4733 m)	63.8	.449	.408	.041	.074	.092	10.9	.048	20.8
Keahole 1000 m off bottom	64.2	.443	.408	.035	.063	.081	12.3	.043	23.1

For explanation of symbols see text.

Acknowledgments

Mr. R. Bartz designed the nephelometer and CTD used in this work. He also carried out the first unsuccessful optical set of measurements. The set of optical and CTD data presented in this report were obtained by Mr. D. Menzies. Their dedication and hard work are greatly appreciated. Initial support for the site survey was provided by the NOAA MUST program. This support was initiated by Dr. Kurt Stehling. Later support came from the University of Hawaii Sea Grant Program. Salary for the Optical Oceanography personnel was provided by the Office of Naval Research through Contract N000 14-67-A-0369-0007 under project NR 083-102. The support of these agencies is hereby gratefully acknowledged.

Mr. M. Allen, Mr. W. Gavenda and Lt. S. Poole, NOAA, assisted in the deep current measurements and data reduction. The current measurements and the geological and geophysical work were supported in part by University of Hawaii Sea Grant College Program under Institutional Grant No. 04-6-158-44114 from NOAA, Office of Sea Grant, Dept. of Commerce. Additional support was provided by the Hawaii Institute of Geophysics and the Marine Affairs Coordinator's Office, State of Hawaii.

## REFERENCES

- Austin, R., and J. Halikas, 1976. The index of refraction of sea water, SIO Ref. No. 76-1, SIO Visibility Laboratory, San Diego.
- Clarke, G.L., and H.R. James, 1939. Laboratory analysis of the selective absorption of light by sea water, J. Opt. Soc. Amer., v. 29, p. 43-55.
- Defant, A., 1961. Physical Oceanography, Vol. I, MacMillan Co., New York, NY, 728 pp.
- Edmond, J.M., Y. Chung and J.G. Sclater, 1971. Pacific Bottom Water: Penetration east around Hawaii. J. Geophys. Res., v. 76, no. 33, p. 8089-8097.
- Ewing, M., and S. Connary, 1970. Nepheloid layer in the North Pacific, in Geological Investigations of the North Pacific, J. Hays, Editor, Geol. Soc. Am. Memoir No. 126.
- Ivanoff, A., 1973. Facteurs physiques, chimiques et biologiques affectant la propagation de la lumière dans les eaux de mer, in Optics of the Sea, AGARD Lect. Ser. No. 61.
- Jerlov, N., 1974. Significant relationships between optical properties of the sea, in Optical Aspects of Oceanography, N. Jerlov and E. Steemann Nielsen, Editors, Academic Press, New York, p. 77-94.
- Jerlov, N., 1976. Marine Optics, Elsevier Publishing Co., Amsterdam, 231 pp.
- Kitchen, J., J. Zaneveld, and H. Pak, 1975. Particle size distributions in a region of coastal upwelling analyzed by characteristic vectors, Limn. and Oceanol., v. 20, no. 5, p. 775-783.
- Lisitsyn, A., 1962. Distribution and Composition of Suspended Materials in Seas and Oceans, U.S.S.R. Academy of Science, Moscow, p. 175-231.
- Mie, G., 1908. Beiträge zue Optik trüber Medien, speziell kolloidalen Metall. lösungen, Ann. Physik, v. 25, p. 377.
- Morel, A., 1973. Diffusion de la lumière par des eaux de mer, in Optics of the Sea, AGARD Lect. Ser. No. 61.
- Nakamura, A. and R. Harvey, 1978. Conversion from film to magnetic cassette recording for the Geodyne 102 current meter. NOAA Tech. Memo, ERL, PMEL-11, 1978. Pacific Marine Environmental Laboratory, Seattle, WA, 15 pp.
- Plank, W., H. Pak, and J. Zaneveld, 1972. Light scattering and suspended matter in nepheloid layers, J. Geophys. Res., v. 77, p. 1689-1694.

- Spinrad, R., J. Zaneveld, and H. Pak, 1978. A comparison of experimental and theoretical values of the volume scattering function of suspended particulate matter at near-forward angles, Applied Optics, April 1978 (in press).
- Sullivan, S.A., 1963. Experimental study of the absorption in distilled water, artificial sea water, and heavy water in the visible region of the spectrum, J. Opt. Soc. Amer., v. 53, p. 962-967.
- Zaneveld, J., 1973. Variation of optical sea parameters with depth, in Optics of the Sea, AGARD Lect. Ser. No. 61.
- Zaneveld, J., 1975. Optical properties of the ocean of concern to DUMAND, in Proceedings of the 1975 DUMAND Summer Workshop, P. Kotzer, Editor, W. Washington State College.
- Zaneveld, J., 1976. Projected optical and particle properties at the DUMAND Maui site, in Proceedings of the 1976 DUMAND Summer Workshop, A. Roberts, Editor, Fermilab, Batavia, Ill., p. 507-516.
- Zaneveld, J., D. Roach, and H. Pak, 1974. Method for the determination of index of refraction distribution of oceanic particulates, J. Geophys. Res., v. 79, no. 27, p. 4091-4095.